



A successive three-point perturbation method for fast ray tracing in complex 2D and 3D geological models



Tao Xu ^{a,*}, Fei Li ^{a,b}, Zhenbo Wu ^{a,b}, Chenglong Wu ^{a,b}, Ergen Gao ^c, Bing Zhou ^d, Zhongjie Zhang ^a, Guoming Xu ^e

^a State Key Laboratory of Lithosphere Evolution, Institute of Geology and Geophysics, Chinese Academy of Sciences, Beijing 100029, China

^b University of Chinese Academy of Sciences, Beijing 100049, China

^c Institute of Disaster Prevention, Sanhe 101601, China

^d Department of Geology and Geophysics, The University of Adelaide, SA 5005, Australia

^e School of Earth and Space Sciences, University of Science and Technology of China, Hefei, 230026, China

ARTICLE INFO

Article history:

Received 10 April 2013

Received in revised form 17 February 2014

Accepted 21 February 2014

Available online 6 March 2014

Keywords:

Three-point perturbation method

Ray tracing

2D and 3D

Block model

Heterogeneous velocity

ABSTRACT

This paper presents new 2D and 3D ray-tracing methods that can be applied to traveltimes and ray path computations for transmitted, reflected and turning seismic waves in complex geologic models. The new ray-tracing scheme combines segmentally iterative ray tracing (SIRT) and pseudo-bending methods to address both stratified and arbitrarily shaped block models. The new method robustly extends our previous constant block models and constant gradient block models to generally heterogeneous block models, and incorporates cubic splines or triangulated interfaces to boundaries of complex geological bodies. The method is thus more widely applicable to practical problems. A successive three-point perturbation scheme is formulated that iteratively updates the midpoints of a segment based on an initial ray path. The midpoints are corrected by applying first-order analytic formulae to locations of the midpoint inside the block or on the boundaries of the blocks, which are then updated with the pseudo-bending method and SIRT algorithm instead of the traditional iterative methods. Empirical applications, including an example addressing the Bohemian Massif, demonstrate that this successive three-point perturbation scheme successfully performs kinematic ray tracing in heterogeneous complex 2D and 3D media.

© 2014 Elsevier B.V. All rights reserved.

1. Introduction

Two-point ray tracing is crucial in locating earthquake, tomographic imaging, seismic migration and design of seismic data acquisition. Compared to the eikonal equation solver (Lan and Zhang, 2013a,b; Vidale, 1988, 1990), two-point ray tracing can calculate both ray-trajectories and traveltimes, which are required in traveltimes tomographic inversions and earthquake source inversion. Dynamic ray tracing can be accomplished by calculating ray amplitudes in terms of the transport equation along the ray-trajectories (Cerveny, 2001). Previously reported kinematic ray-tracing techniques include shooting methods (Langan et al., 1985; Sambridge et al., 1995; Sun, 1993; Virieux and Farra, 1991; Xu et al., 2008) and bending methods (Aki and Richards, 1980; Julian and Gubbins, 1977; Keller and Perozzi, 1983; Mao and Stuart, 1997; Pereyra, 1992; Prothero et al., 1988; Thurber and Ellsworth, 1980; Um and Thurber, 1987; Xu et al., 2006, 2010). Shooting methods are efficient in global search for receivers, whereas bending methods are advantageous in case of high uncertainty in functions relating receiver positions and shooting angles. Other methods include

wave-front techniques (Vinje et al., 1993, 1996), the shortest path methods (Moser, 1991; Zhang et al., 2000; Zhao et al., 2004) and simulated annealing search (Velis and Ulrych, 1996, 2001). The most advantage of the three methods is to trace a global minimum of the traveltimes. A good review of these methods can be found in Cerveny (2001, 1988).

The ray-tracing methods described above are all based on model parameterizations, which may be defined by either a set of discrete velocity values (Langan et al., 1985; Moser, 1991; Vidale, 1988, 1990) or a piecewise set of continuous velocity functions (Chapman and Pratt, 1992; Zhou and Greenhalgh, 1992a,b). Rectangular cells perform better than irregular cells in the grided-models in calculating traveltimes and tracking ray paths. The complex geometries of natural geological media require fine-scale grids that can become computationally intensive, especially in processing three-dimensional models (Moser, 1991; Zhao et al., 2004).

Kinematic as well as dynamic ray-tracing methods often employ continuous parameterization operations, which may solve eikonal and transportation equations, and improve the accuracy of traveltimes and amplitude estimates. Layered structures are widely used in this circumstance and may be characterized by sequential continuous media (GuiZiou et al., 1996; Keller and Perozzi, 1983; Mao and Stuart, 1997; Rawlinson et al., 2001; Zelt and Smith, 1992; Zhang and Klemperer,

* Corresponding author. +86 10 82998313.

E-mail address: xutao@mail.iggcas.ac.cn (T. Xu).

2005; Zhang and Wang, 2007; Zhang et al., 2003, 2005, 2013). A horizontally stratified model for example provides the most efficiently calculated traveltimes and ray paths for sedimentary material. The ray-tracing algorithm for layered model however does not apply to the complex subsurface media often encountered in seismic exploration, which instead resembles a series of irregular blocks. An irregular block model can more accurately approximate complex structures such as faults, pinch-out layers, intrusive bodies and lenses, but also brings more computational times of ray-tracing in such complex geological models (Bai et al., 2007; Gjøystdal et al., 1985; Pereyra, 1992, 1996; Xu et al., 2006, 2010).

We recently developed a robust segmentally iterative ray tracing (SIRT) method in an irregular block model. Two fast ray-tracing algorithms have been proposed for the constant velocity block model (Xu et al., 2006) and constant velocity gradient block model (Xu et al., 2010). This paper, extends our previous work by applying SIRT method to a heterogeneous block model that more closely approximates geological media. The extension required (1) model parameterization with generally heterogeneous velocity blocks and arbitrary boundaries defined by cubic splines or triangulated interfaces, (2) analytic formulations of the ray bending for velocity blocks and boundaries, and (3) successive three-point optimization of ray tracing. We applied the new method to several 2D and 3D geological models to demonstrate its capability and computational efficiency in practical applications.

2. Model parameterization

2.1. Block models

Two- and three-dimensional geological structures were discretized in a three-step procedure following previous methods (Xu et al., 2006, 2008, 2010). We first divide the model domain into non-overlapping sub-domains that represent different geological units or blocks. Second, we approximate boundaries of the blocks using cubic spline interpolation or triangulated interfaces. Finally, we calculate the velocity of each block using the spatial coordinates bounded by the cubic spline interpolations or triangulated surfaces (see examples given by Figs. 1 and 2).

In the 3D case, triangulated interface methods can more accurately match the geometry of geological media and trace rays more efficiently than the B-spline surface patches, i.e. the discrete points are not necessary to be defined in a rectangular domain, no gaps would be produced in linking triangulated patches whereas strict constraints are requisite in B-spline linking, and thus facilitates the modification or elimination of nodes that is necessary in approximating complex geological structures. Furthermore, the intersection between a line and a triangle can

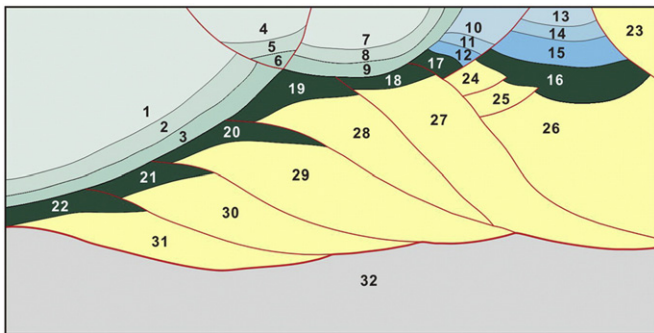


Fig. 1. 2D block model (Model 1) representing the geological characteristics of a fore-land nappe structure along the edge of compressional basin. Different structural elements are shown in different colors separated by cubic splines. This geological situation does not lend itself to standard layer parameterization.

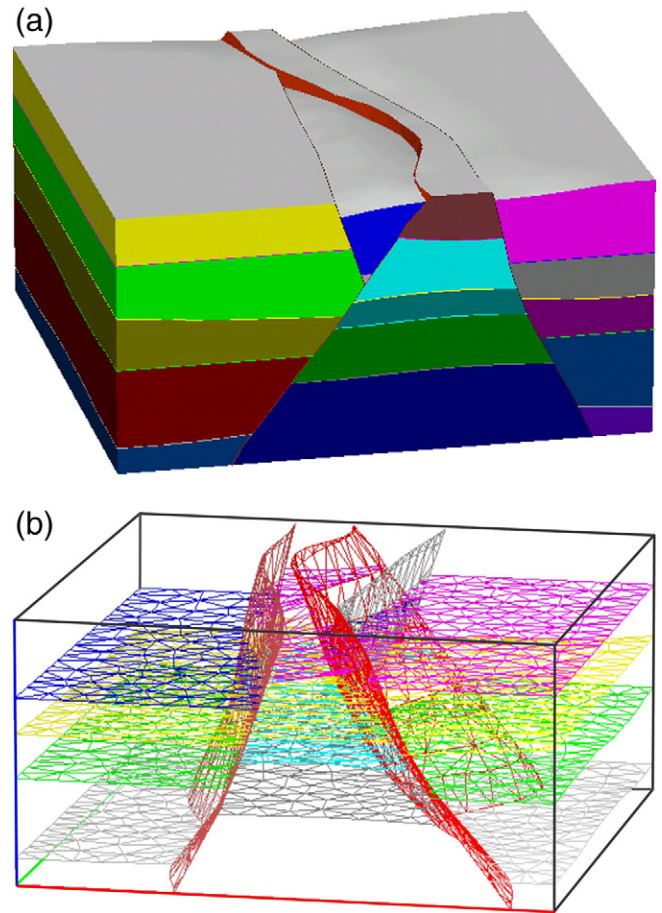


Fig. 2. Model 2, representing horst structures, includes several different blocks, shown in different colors (a) and separated by triangulated interfaces (b).

be directly computed whereas identification of ray/B-spline patch intersection requires iterative modeling (Rawlinson et al., 2001; Virieux and Farra, 1991). Hence large numbers of ray/interface intersections can be computed quickly to save tracing time.

Triangulated interfaces have been applied in the well-known GOCAD system (Mallet, 1989, 1992). The drawback of this technique is that it generates rougher surfaces than those generated by B-spline interpolation. Normal vectors held constant within a given triangle will vary abruptly in the boundary region between two triangles that are not in the same plane. A reflected or transmitted ray may abruptly change direction at these boundaries. This situation poses challenges for ray tracing methods that rely on nearby smooth ray trajectories for an optimal solution. To address this problem, we developed an algorithm that redefines normal vectors at arbitrary points on an interface in such a way that renders them continuous on the whole interface (Xu et al., 2006). Figs. 1 and 2 show two geological models that are discretized by this block discretization technique.

Model 1 (Fig. 1) represents a fore-land nappe structure on the periphery of a compressional basin. The Longmenshan and the Dabashan fore-land thrust belts of the Sichuan basin and those around the Tarim basin in China are examples of this type of geological setting. The regional model contains 32 elements, 97 edges and 245 points.

Model 2 (Fig. 2a) represents horst and graben structures in an extensional basin. These structures are common among basins found in the eastern China, including the Bohai Sea and the Subei and Songliao basins. The 3D model contains 18 blocks, 6676 triangles and 2700 points.

Note that Fig. 2b illustrates several triangulated interfaces within the model.

2.2. Velocity distribution within a block

Velocities within blocks may be defined by a constant or constant gradient (Rawlinson et al., 2001; Slotnick, 1936; Xu et al., 2010), by exponential increase (Slotnick, 1936), by conic function (Ravve and Koren, 2007) or other typical functions (Al-Chalabi, 1997) according to the real-world medium they approximate. In order to inform general applications, we expressed block velocities as the following trilinear interpolation (Thurber, 1983):

$$v(x, y, z) = \sum_{l=0}^1 \sum_{m=0}^1 \sum_{n=0}^1 v(i+l, j+m, k+n) \left(1 - \frac{|x-x_{i+l}|}{|x_{i+1}-x_i|}\right) \times \left(1 - \frac{|y-y_{j+m}|}{|y_{j+1}-y_j|}\right) \left(1 - \frac{|z-z_{k+n}|}{|z_{k+1}-z_k|}\right) \quad (1)$$

where, $v(i+l, j+m, k+n)$ are velocity values at the eight points surrounding a given point (e.g., point $P(x, y, z)$ in Fig. 3). Eq. (1) ensures that the velocity field is continuous throughout the block, even though the velocity gradient will be discontinuous from cell to cell. Velocity distributions in different blocks are defined according to different sets of velocity grid points. Applying Eq. (1), we can calculate the velocity at any point in the block model.

3. Ray tracing method

The segmentally iterative ray tracing (SIRT) method finds the optimal traveltimes by perturbing intersection points on the interfaces along a ray path across a constant block (Xu et al., 2006) or a constant gradient of blocks (Xu et al., 2010). Both approaches are essentially three-point perturbation schemes, as well as pseudo-bending ray-tracing algorithms (Um and Thurber, 1987). To extend the method, we adapted the previous SIRT and pseudo-bending methods to heterogeneous blocks whose velocities are given by Eq. (1). The new version of SIRT formulates the updating schemes for the perturbed midpoints in terms of their location inside blocks or along interfaces.

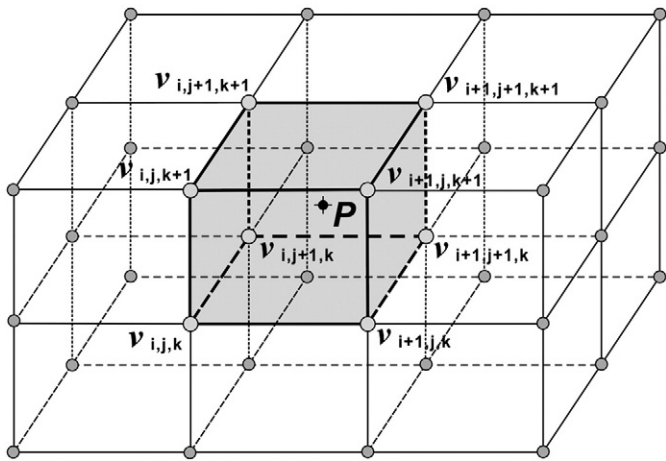


Fig. 3. The velocity field for each block is defined as a grid with a discrete set of velocity nodes. A trilinear interpolation function is used to calculate the velocity at any point $P(x, y, z)$ according to velocity values at the eight grid points surrounding point P .

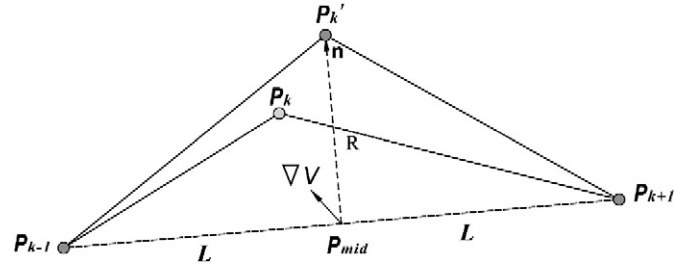


Fig. 4. Illustration of the three-point perturbation scheme and pseudo-bending methods used to address a midpoint located inside of a given model block.

3.1. Midpoint modification within a block

Due to its efficiency for two-point ray tracing, we adopted the pseudo-bending scheme of Um and Thurber (1987), in which an initial path is estimated and then perturbed by a geometric interpretation of ray equations. The method then minimizes a piecewise function to identify optimal traveltimes along the path by minimizing a piecewise fashion. Assuming successive points along a ray path, P_{k-1}, P_k, P_{k+1} with coordinates x_{k-1}, x_k, x_{k+1} (Fig. 4), and two fixed end-points, P_{k-1} and P_{k+1} , we then search for a new midpoint P'_k to replace the previous P_k , which gives the minimal traveltimes along the new ray path P_{k-1}, P'_k, P_{k+1} . The modifications include the directional vector \mathbf{n} and distance R (Fig. 4) calculated by the following formulae (Um and Thurber, 1987)

$$\mathbf{n}' = \nabla_{P_k} V - \left[\nabla_{P_k} V \cdot (x_{k+1} - x_{k-1}) \right] \frac{x_{k+1} - x_{k-1}}{|x_{k+1} - x_{k-1}|^2},$$

$$\mathbf{n} = \frac{\mathbf{n}'}{|\mathbf{n}'|}$$

$$R = -\frac{cV_{mid} + 1}{4\mathbf{cn} \cdot \nabla_{P_{mid}} V} + \sqrt{\frac{(cV_{mid} + 1)^2}{(4\mathbf{cn} \cdot \nabla_{P_{mid}} V)^2} + \frac{L^2}{2cV_{mid}}} \quad (2)$$

where, $L = |x_{k+1} - x_{mid}|$, $c = (1/v_{k+1} + 1/v_{k-1})/2$, $\nabla_{P_k} V$ is the velocity gradient with respect to the midpoint P_k , V_{mid} is the velocity of central point P_{mid} with coordinate x_{mid} and $\nabla_{P_{mid}} V$ is the velocity gradient at the point P_{mid} .

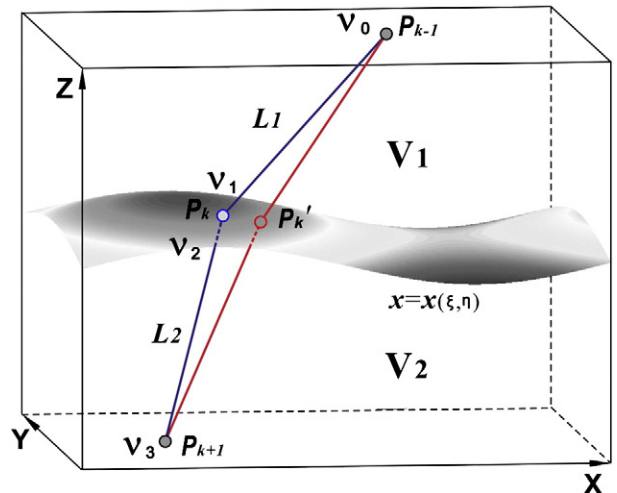


Fig. 5. Illustration of the three-point perturbation scheme and segmentally-iterative methods used to address a midpoint located along a model block interface.

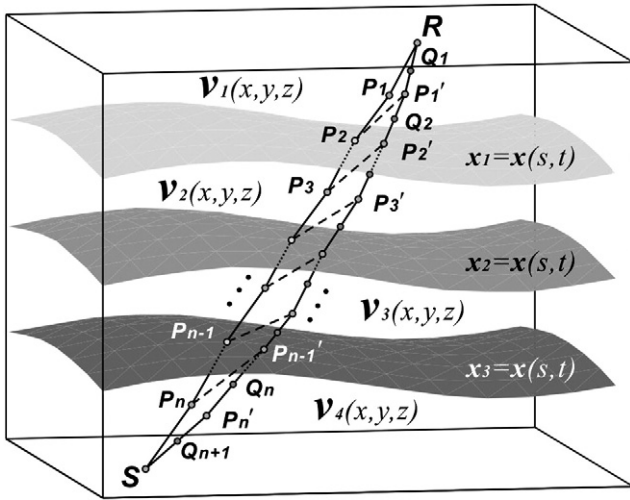


Fig. 6. Sketch of the three-point perturbation scheme for ray tracing in a generalized heterogeneous media.

3.2. Midpoint modification along interfaces

Applying Fermat's principle, we derive a general approximate formula for modifying the intersection points linking two heterogeneous velocities. As shown in Fig. 5, P_{k-1}, P_k, P_{k+1} are three successive points

points of intersection along a ray trajectory. Coordinates of the midpoint P_k on the surface are given as a function of two parameters, ξ and η :

$$x_k = x_k(\xi, \eta) \tag{3}$$

Given fixed P_{k-1} and P_{k+1} , and assuming only short distances between the three points P_{k-1}, P_k and P_{k+1} , the traveltime can be expressed as a function of the midpoint coordinates $x_k(\xi, \eta)$

$$T = t_1(P_{k-1}, x_k) + t_2(x_k, P_{k+1}) \tag{4}$$

or

$$T = |x_k - x_{k-1}|(1/v_0 + 1/v_1)/2 + |x_{k+1} - x_k|(1/v_2 + 1/v_3)/2 \tag{5}$$

These equations differ from our previous formulae for constant blocks (Xu et al. 2006) and constant gradient blocks (Xu et al. 2010). The stationary traveltime satisfies the zero partial derivative at the improved midpoint $(\xi + \Delta\xi, \eta + \Delta\eta)$, i.e.

$$\left. \frac{\partial T}{\partial \xi} \right|_{(\xi=\xi+\Delta\xi, \eta=\eta+\Delta\eta)} = 0, \quad \left. \frac{\partial T}{\partial \eta} \right|_{(\xi=\xi+\Delta\xi, \eta=\eta+\Delta\eta)} = 0. \tag{6}$$

Using the first term of a Taylor series, Eq. (6) become

$$\frac{\partial T}{\partial x_i} x_{i\xi} + \left(\frac{\partial^2 T}{\partial x_i \partial x_j} x_{i\xi} x_{j\xi} + \frac{\partial T}{\partial x_i} x_{i\xi\xi} \right) \Delta\xi + \left(\frac{\partial^2 T}{\partial x_i \partial x_j} x_{i\xi} x_{j\eta} + \frac{\partial T}{\partial x_i} x_{i\xi\eta} \right) \Delta\eta = 0,$$

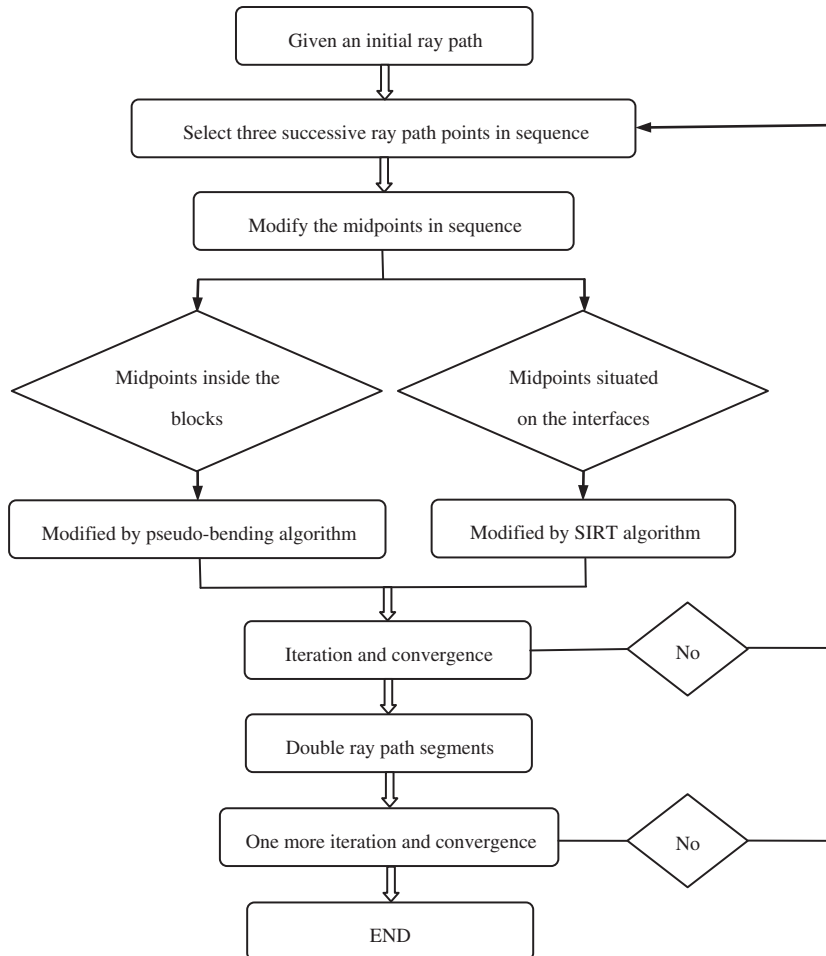


Fig. 7. Flow chart describing the three-point perturbation scheme for ray tracing.

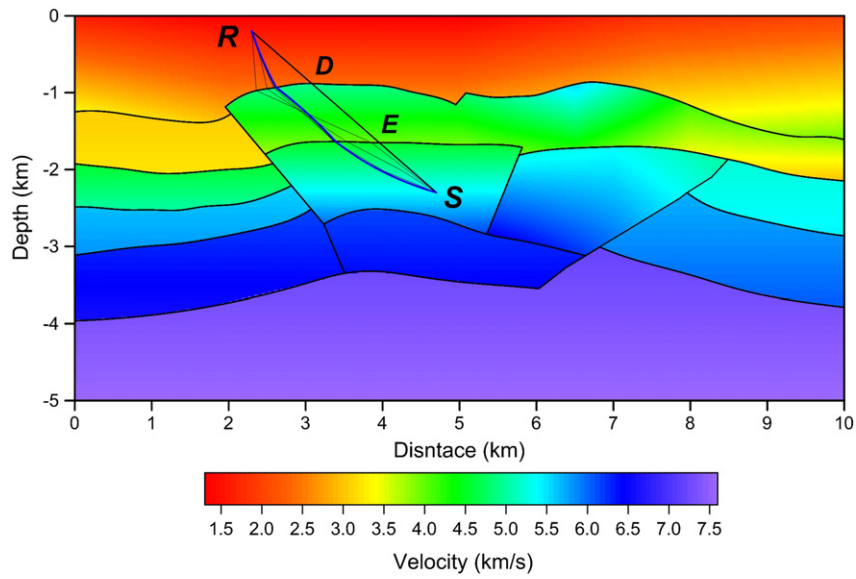


Fig. 8. Illustration of the sequence of ray paths following their perturbation from an initial ray path *RDES*. The velocity distribution approximates that of central uplift zones found in compressional basins (Model 3). The thick blue line is the final ray path after several iterations of the method.

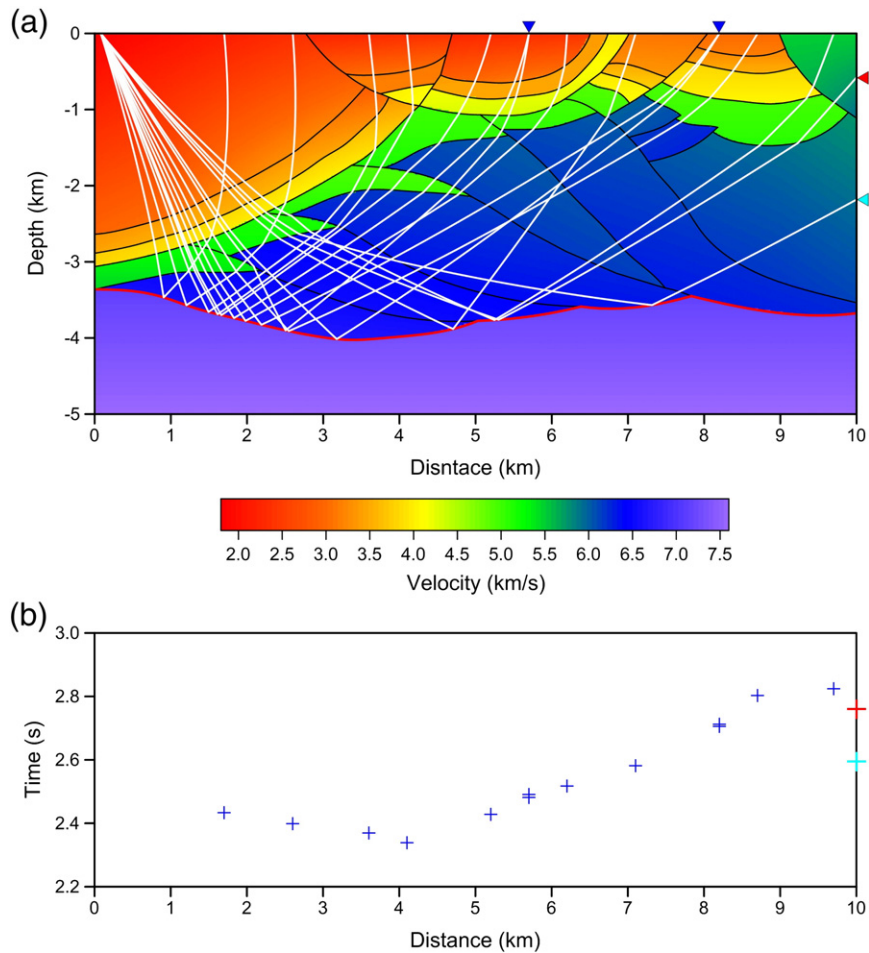


Fig. 9. (a) Ray tracing results for the Model 1 velocity distribution. Surface receivers (blue triangles at the surface) trace multiple paths while subsurface receivers trace two ray paths (red and teal triangles along the right boundary). (b) Calculated traveltimes marked with crosses.

$$\frac{\partial T}{\partial x_i} x_{in} + \left(\frac{\partial^2 T}{\partial x_i \partial x_j} x_{in} x_{j\epsilon} + \frac{\partial T}{\partial x_i} x_{in\epsilon} \right) \Delta \xi + \left(\frac{\partial^2 T}{\partial x_i \partial x_j} x_{in} x_{j\eta} + \frac{\partial T}{\partial x_i} x_{in\eta} \right) \Delta \eta = 0, \quad (7)$$

where the subscript i refers to the three coordinates of the midpoint. The two parameter perturbations are calculated following (Xu et al., 2006, 2010)

$$\Delta \xi = \frac{U_{13}U_{22} - U_{23}U_{12}}{U_{11}U_{22} - U_{12}U_{21}}, \Delta \eta = \frac{U_{11}U_{23} - U_{21}U_{13}}{U_{11}U_{22} - U_{12}U_{21}}, \quad (8)$$

where

$$\begin{aligned} U_{11} &= \frac{\partial^2 T}{\partial x_i \partial x_j} x_{i\epsilon} x_{j\epsilon} + \frac{\partial T}{\partial x_i} x_{i\epsilon\epsilon}, U_{12} = \frac{\partial^2 T}{\partial x_i \partial x_j} x_{i\epsilon} x_{j\eta} + \frac{\partial T}{\partial x_i} x_{i\epsilon\eta}, U_{13} = -\frac{\partial T}{\partial x_i} x_{i\epsilon}, \\ U_{21} &= \frac{\partial^2 T}{\partial x_i \partial x_j} x_{in} x_{j\epsilon} + \frac{\partial T}{\partial x_i} x_{in\epsilon}, U_{22} = \frac{\partial^2 T}{\partial x_i \partial x_j} x_{in} x_{j\eta} + \frac{\partial T}{\partial x_i} x_{in\eta}, U_{23} = -\frac{\partial T}{\partial x_i} x_{in}, \\ x_{i\epsilon} &= \frac{\partial x_i}{\partial \xi}, x_{in} = \frac{\partial x_i}{\partial \eta}, x_{i\epsilon\epsilon} = \frac{\partial^2 x_i}{\partial \xi^2}, x_{i\epsilon\eta} = x_{in\epsilon} = \frac{\partial x_i \partial x_j}{\partial \xi \partial \eta}, x_{in\eta} = \frac{\partial^2 x_i}{\partial \eta^2}. \end{aligned} \quad (9)$$

Substituting average slownesses

$$\frac{1}{V_1} = \frac{1/v_0 + 1/v_1}{2}, \frac{1}{V_2} = \frac{1/v_2 + 1/v_3}{2} \quad (10)$$

for constant slownesses $1/V_1$ and $1/V_2$ (see Fig. 5) in the updating procedure outlined above produces no difference in the constant velocity (Xu et al., 2006).

The above formulations show that the perturbation formulae are all explicit, first-order operations rather than iterative approaches like the bisection method (Zhao et al., 1992). Since ray tracing schemes modify millions of intersection points, the explicit, first-order versions facilitate ray tracing in complex geological models by directly substituting the position $(\xi + \Delta \xi, \eta + \Delta \eta)$ for the primary position (ξ, η) if the updated midpoint falls on the same interface as that of its predecessor. If not, further analysis can determine whether intersection points should be added or removed (Xu et al., 2006, 2010).

3.3. Three-point perturbation method of ray tracing

To implement ray-tracing in the heterogeneous block model, we combine the pseudo-bending scheme and SIRT algorithm into a new three-point ray tracing method that gives a ray path of transmitted wave (Fig. 6). The initial ray path connects a shot S , and a receiver R , through the points $P_1 P_2 P_3 \dots P_{n-1} P_n$ (see Fig. 6), where odd numbered points $P_1 P_3, \dots, P_n$ are located within the blocks and even numbered points $P_2 P_4, \dots, P_{n-1}$ fall along boundary interfaces. Using the initial three points $R P_1 P_2$, we applied Eq. (2) or Eq. (8) to update the midpoint P_1 within the block or along the boundary interface. This correction provides a new midpoint P'_1 , which gives the minimal traveltime from R to P_2 . Repeating this processing with a new triplet of points (e.g., $P'_1 P_2 P_3$) gives a new midpoint P'_2 . This midpoint correction process continues until the end point S is reached, rendering a new ray path that connects the points $R P'_1 P'_2 P'_3 \dots P_n - \{P'_n S$. The same process may be repeated several times to obtain the most accurate ray path for a precision of 1 m in a $5 \times 5 \times 5$ km model. Then we should double ray path segments by interpolating new points that form the convergent ray path $R P'_1 P'_2 P'_3 \dots P_n - \{P'_n S$. This procedure interpolates point Q_1 as the midpoint of R and P'_1 , and point Q_2 as the midpoint of P'_1 and P'_2 and so forth, to produce new ray path $R Q_1 P'_1 Q_2 P'_2 \dots Q_n P'_n Q_{n+1} S$. If the ray path converges with an additional iteration, then the ray tracing terminates. Otherwise, the procedure continues until desired precision is reached.

In the above procedure, some points are inside of the blocks, requiring that we double the segments by interpolating new points (Um and Thurber, 1987). Because Eq. (5) implies weak heterogeneity, we must reduce the length of the segment by interpolating new points in order to address the assumed properties of weakness. In cases of pronounced heterogeneity, we iteratively upgrade parameters estimated by the formula until reaching the expected accuracies. Fig. 7 shows the ray-tracing procedure in flow chart form. As shown in the flow chart, each shot/receiver pair requires an initial ray path that is often obtained by shooting methods. Shooting scheme however can be computationally intensive in a heterogeneous velocity model. Here, we simply use straight lines as the initial ray paths. It should be noted that if the receiver is located in the shadow zone, the ray path will not converge during iterations, or may converge to a local minima.

4. Numerical experiments

To illustrate the new ray-tracing method, we conducted seismic ray-tracing using specific 2D and 3D geological models. These results demonstrated the method's ability to determine the paths of transmitted, reflected and turning waves.

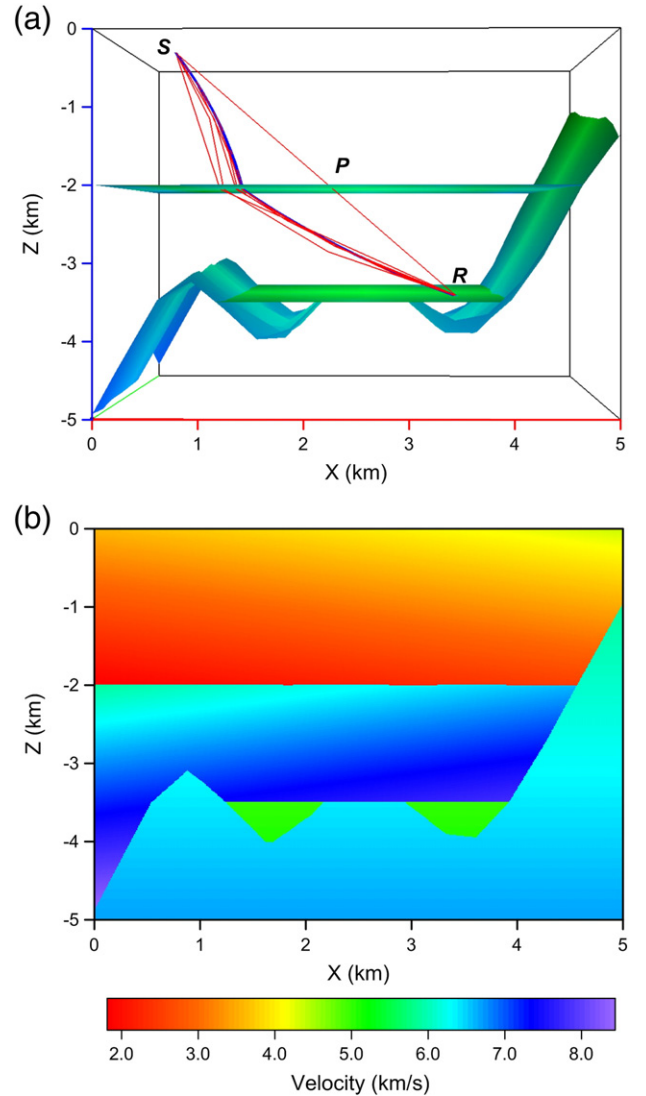


Fig. 10. (a) Illustration of the sequence of ray paths following perturbation from a three-point initial path SPR in model showing cross-cutting relationships in a layered media (Model 4). (b) Velocity distribution at the position $y = 2.5$ km.

4.1. 2D cases

Model 3 (Fig. 8) is designed to reflect central uplift zones within a compressional basin (e.g., the Tazhong uplift zone of the Tarim basin, China). The uplift zone typically results from peri-compressional modification of the basin and produces horst structures generated by small-scale thrust faults. The model contains 12 elements, 41 edges and 128

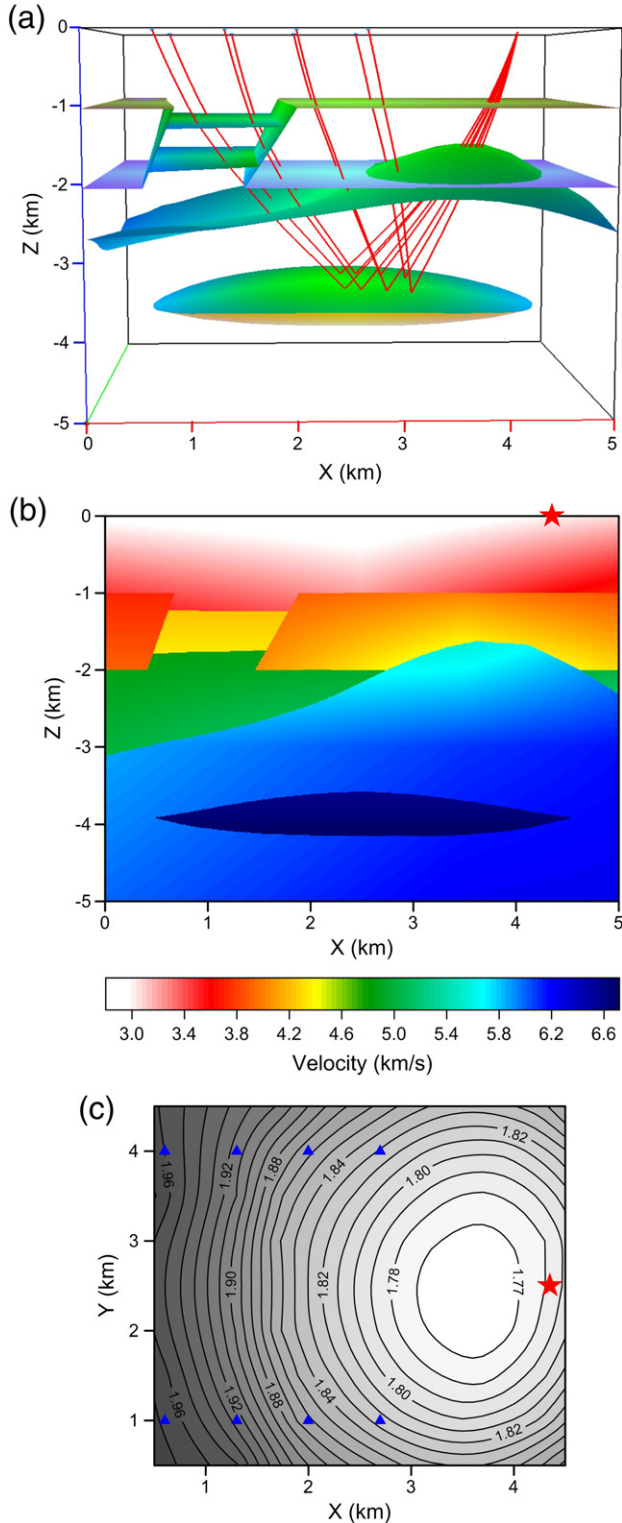


Fig. 11. (a) 3D ray tracing results for Model 5, which consists of variable velocity distributions for different blocks. (b) Velocity distribution at the position $y = 2.5$ km. (c) Calculated traveltimes isolines.

points. Shot position S and receiver R are connected by a straight line (initial ray path), which intersects the interfaces at point D and E. Fig. 8 illustrates the ray path iterations perturbed from the initial ray path, $RDES$, associated with the velocity distribution. The thick blue line represents the ultimate ray path after several iterations.

Fig. 9a shows the ray-tracing results of a shot with the velocity distribution given in Model 1. The computed traveltimes are given in Fig. 9b. The thick red line in Fig. 9a indicates the reflector for traveltimes in Fig. 9b. Note that the two receivers traced multiple paths marked along the surface as blue triangles. Associated traveltimes errors can also be distinguished. We also show two ray paths traced to subsurface receivers, marked with red and teal triangles on the right boundary. The red and teal crosses represent traveltimes (Fig. 9b), which can help constrain well logging activities.

4.2. 3D cases

Model 4 (Fig. 10a) is designed to represent cross-cutting and superposition in a complex geologic medium. The model consists 5 blocks, 3635 triangles and 1681 points. Fig. 10b shows a cross-section of the 3D velocity distribution at position $y = 2.5$ km. The initial ray path (straight line) connects shot position S and receiver R, and goes on to

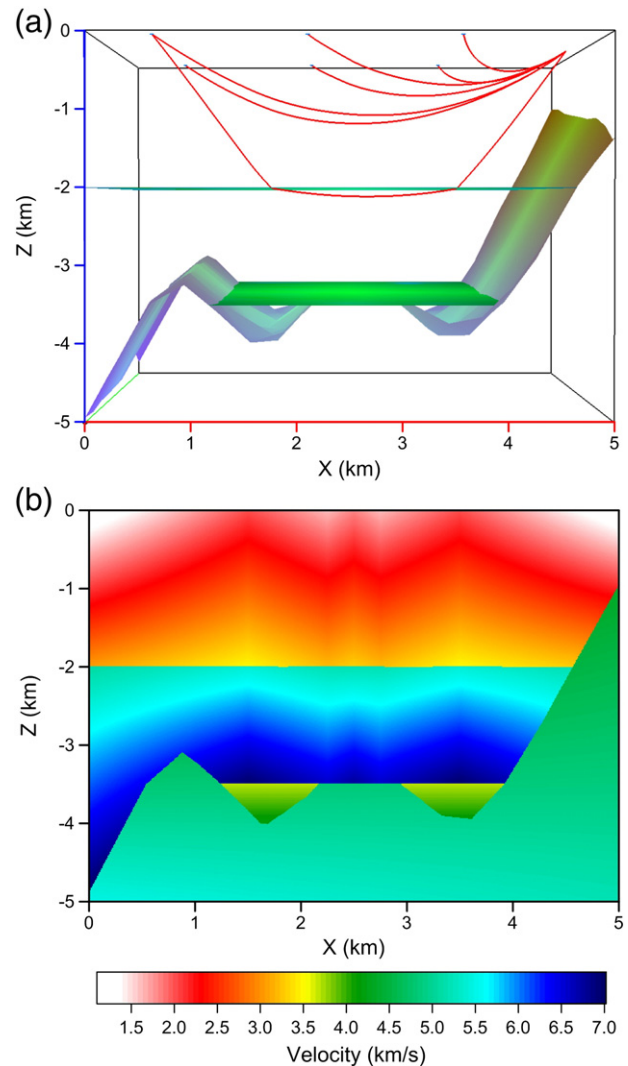


Fig. 12. (a) Ray-tracing results for turning waves in the layered cross-cutting model (Model 4). (b) Velocity distribution at the position $y = 2.5$ km.

intersect the interface at point *P*. Fig. 10a illustrates the sequences of ray paths as they are perturbed from initial ray path *SPR*. The thick blue line shows the final ray path after several iterations.

Model 5 (Fig. 11) represent a magmatic intrusion into country rock, assuming differentiation within the magma itself. When the magma intrudes overlying country rocks, it usually causes faulting of the host rock and the formation of an extensional dome. Magmatic differentiation resulting from fractional crystallization can generate zonation of plutons and other intrusive bodies having different compositions and densities, as well as metal-rich porphyries. Model 5, with a size of $5 \times 5 \times 5$ km, consists of normal faults, reverse faults, an intrusive mass and a lens. The model includes 7 blocks, 4649 triangles and 2152 points. Fig. 11b shows a cross-section of the 3D velocity distribution at position $y = 2.5$ km. The upper interface of the lens is defined as the reflecting interface. Fig. 11a shows the tracing results and traveltimes in the (x, y)-plane. For the sake of clarity, only eight ray paths from the shot are shown. The shot position and eight receivers are marked as the red star and blue triangles, respectively in Fig. 11c.

Model 4 demonstrates the tracing of a turning ray in another velocity distribution (Fig. 12b). The 3-D model is the same as that shown in Fig. 10. Seven turning rays from the tracing results are shown in Fig. 12a.

To determine tracing speed, we assumed a single source and 800 receivers positioned throughout a 20×40 surface grid. The CPU time (Centrino-2, 2.53 GHz) to execute SIRT in Model 5 with a precision of 0.25 m was 9.74 s. The shooting method required an additional 14.62 s and gave a precision of 0.5 m. These computational times demonstrate the efficiency of the three-point perturbation method under these conditions. Note that the precision of the three-point perturbation method is defined by the largest modifying distance along the perturbed trajectory, whereas precision of the shooting method is defined by the distance between positions of the receiver and the emergence point.

4.3. Analyzing crustal and uppermost mantle structure of the Bohemian Massif using CELEBRATION 2000 data

Specific model parameterizations make it difficult to compare the adaptive capabilities of various ray-tracing methods. We applied our ray-tracing method to the crustal and uppermost mantle structure of

the Bohemian Massif using CELEBRATION 2000 data (Hrubcova et al., 2005), to determine its suitability for empirical seismic imaging. The Bohemian Massif includes several tectonic units separated by faults, shear zones or thrusts, and is further described in Babuska and Plomerova (2013), Faryad et al. (2013), Hajna et al. (2011), and Maierova et al. (2014). The velocity profile was obtained by two-dimensional trial-and-error forward modeling of seismic waves, using the Seis83 software package (Cerveny and Psencik, 1984).

There is no difficulty when a stratified velocity model used in program packages of Seis83 and Seis88 (Cerveny and Psencik, 2002) is redescribed by a block model. The 2D model interfaces are described by cubic splines in both the Seis83 and Seis88 velocity models and in the models assumed in this paper. Given identical velocity distributions from shared interpolation methods, the two methods should calculate same way tracing results and traveltimes.

We constructed a block velocity model using data presented in Hrubcova et al. (2005), shown in Fig. 13. Hrubcova et al. (2005) used bi-cubic interpolation to derive the velocities between points whereas this report used bi-linear interpolation. There are some differences in the velocity values for profiles derived by the two methods (e.g., an obvious difference appears in the uppermost mantle at around 250 km along the horizontal axis and 45 km depth). Fig. 14 shows ray-tracing results calculated here superimposed over traveltimes for SP 29060 reported in Hrubcova et al. (2005). The blue segments represent traveltimes calculated by Seis83, and the red crosses give results calculated by the ray-tracing method described above. The two traveltimes match quite well except in a few cases for which the two methods interpolated differences in the velocity values.

The complex geological models shown in Figs. 8 and 9 lend themselves to block model representation but not to 2D layer structure options in Seis83 and Seis88. The layered model options in the ANRAY 3D seismic package (e.g., Psencik and Teles, 1996) would also not suffice in describing the complex 3D geological models addressed here (e.g., Figs. 2, 10 and 11). Seis83, Seis88 and ANRAY do not offer accurate ray tracing for complex 2D and 3D models, nor do they provide adequate earthquake location, tomography and seismic migration for more complex geological settings. Model parameterization methods described in this paper and in previous works (Xu et al., 2006, 2010), along with

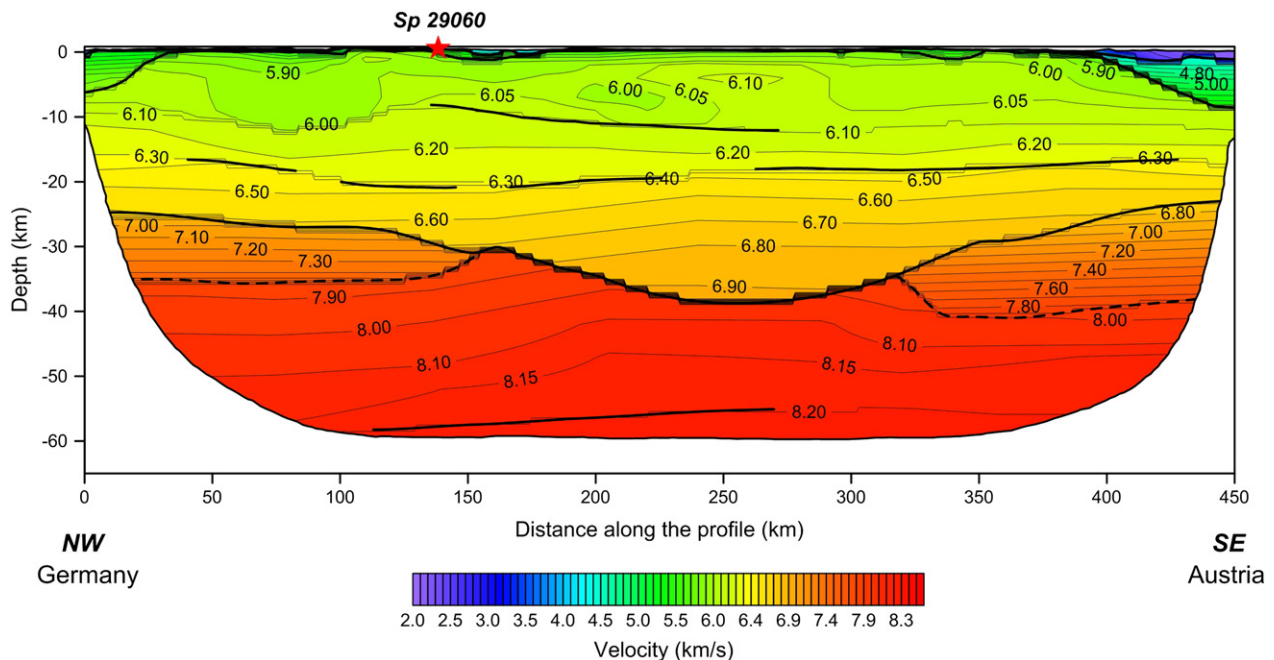


Fig. 13. Velocity model for the crust and uppermost mantle of the Bohemian Massif as derived from CELEBRATION 2000 data (Hrubcova et al., 2005; Fig. 6).

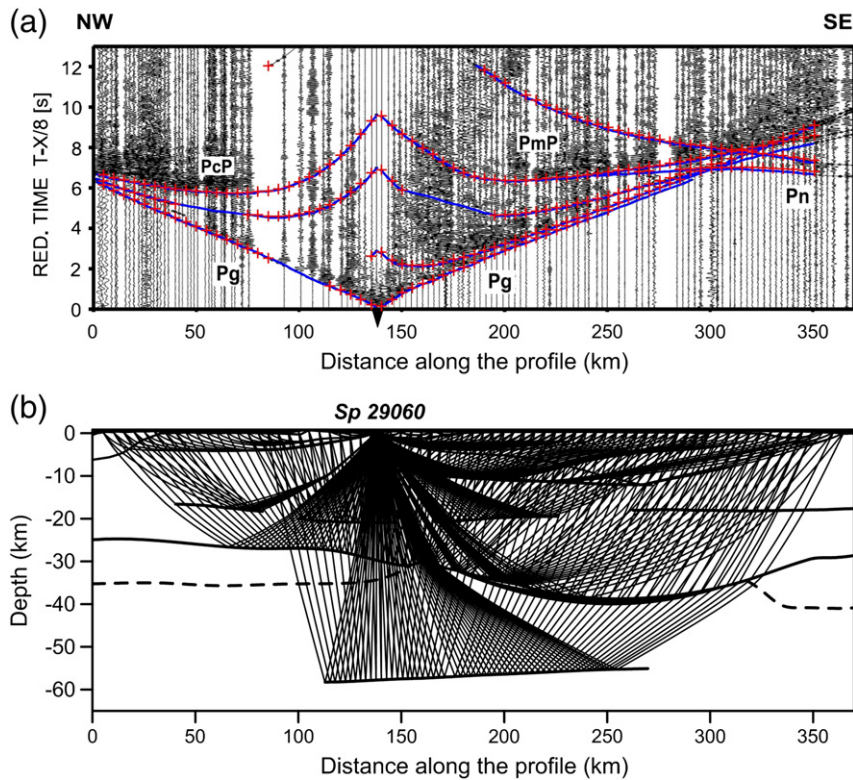


Fig. 14. Ray tracing results (b) and calculated traveltimes (a) for subsurface structure SP 29060 (Fig. 7a in Hrubcova et al., 2005). The blue line segments denote traveltimes calculated by Seis83 seismic software, and the red crosses denote traveltimes calculated by our ray tracing method.

more detailed velocity field information, make it possible to image complex 3D structures with greater accuracy and detail.

5. Conclusions

We adapted our previous SIRT seismic ray-tracing method to laterally heterogeneous block models, in which block velocity shows spatial variation similar to that observed in complex geological settings. The developments of the SIRT ray-tracing algorithm include a successive three-point perturbation scheme that combines the previous SIRT and pseudo-bending methods for generally heterogeneous block models. Experiments with hypothetical 2D and 3D models demonstrate the method's capabilities and efficiency in calculating traveltimes and ray paths of transmitted, reflected and turning waves in complex geological media.

The new method applies a more general description of velocity distributions and a highly efficient ray-tracing algorithm in modeling complex geological settings. These capabilities represent its primary advantages over standard seismic software packages (e.g., Seis83, Seis88 and ANRAY). The new method can also perform forward modeling steps of earthquake location, sub-surface tomography and depth migration in seismic analysis. The primary limitation of the current version of this method is that ray tracing derives from the first arrivals of a single wave mode, i.e. P- or S-wave reflections, refractions and transmissions.

Acknowledgments

We gratefully acknowledge the financial support of the Ministry of Land and Resources of China (SinoProbe-03-02, SinoProbe-02-02), the Ministry of Science and Technology of China (2011CB808904), the Chinese Academy of Sciences (XDB03010700) and the National Natural Science Foundation of China (41021063, 40930418, 41174075, and 41174043). We thank Dr. P. Hrubcova from the Geophysical Institute,

Academy of Sciences of the Czech Republic, for providing the Bohemian Massif velocity model for method comparison. Prof. Fuqin Zhang and Dr. Laicheng Miao provided helpful discussions and feedback that improved the quality of this work.

References

- Aki, K., Richards, P.G., 1980. *Quantitative Seismology: Theory and Methods*. W.H. Freeman and Co., New York.
- Al-Chalabi, M., 1997. Time–depth relationships for multiplayer depth conversion. *Geophys. Prospect.* 45, 715–720.
- Babuska, V., Plomerova, J., 2013. Boundaries of mantle–lithosphere domains in the Bohemian Massif as extinct exhumation channels for high-pressure rocks. *Gondwana Res.* 23 (3), 973–987.
- Bai, C.Y., Greenhalgh, S.A., Zhou, B., 2007. 3D ray tracing by an irregular shortest path method. *Geophysics* 72, T27–T36.
- Cerveny, V., 2001. *Seismic Ray Theory*. Cambridge University Press.
- Cerveny, V., Psencik, I., 1984. SEIS83—numerical modelling of seismic wave fields in 2-D laterally varying layered structures by the ray method. In: Engdall, E.R. (Ed.), *Documentation of Earthquake Algorithms*. World Data Cent. A for Solid Earth Geophys, Boulder, Colo, pp. 36–40 (Rep. SE-35).
- Cerveny, V., Psencik, I., 2002. Ray-theory amplitudes and synthetic seismograms in 2-D inhomogeneous isotropic layered structures. Program package SEIS. *Seismic Waves in Complex 3-D Structures*, Report 12. Dep. Geophys. Charles Univ, Prague, pp. 53–65.
- Cerveny, V., Klimes, L., Psencik, I., 1988. Complete seismic-ray tracing in three-dimensional structures. In: Doornbos, D.J. (Ed.), *Seismological Algorithms*. Academic Press, New York, pp. 89–168.
- Chapman, C.H., Pratt, R.G., 1992. *Traveltime tomography in anisotropic media*. I. Theory. *Geophys. J. Int.* 109, 1–19.
- Faryad, S.W., Jedlicka, R., Ettinger, K., 2013. Subduction of lithospheric upper mantle recorded by solid phase inclusions and compositional zoning in garnet: example from the Bohemian Massif. *Gondwana Res.* 23 (3), 944–955.
- Gjøystdal, H., Reinhardsen, J.E., Astebol, K., 1985. Computer representation of complex 3-D geological structures using a new “solid modeling” technique. *Geophys. Prospect.* 33, 195–211.
- GuiZiou, J.L., Mallet, J.L., Madariaga, R., 1996. 3-D seismic reflection tomography on top of the GOCAD depth modeler. *Geophysics* 61 (5), 1499–1510.
- Hajna, J., Zak, J., Kachlik, V., 2011. Structure and stratigraphy of the Teplá-Barrandian Neoproterozoic, Bohemian Massif: a new plate-tectonic reinterpretation. *Gondwana Res.* 19 (2), 495–508.

- Hrubcova, P., Sroda, P., Spicak, A., Guterch, A., Grad, M., Keller, G.R., Brueckl, E., Thybo, H., 2005. Crustal and uppermost mantle structure of the Bohemian Massif based on CELEBRATION 2000 data. *J. Geophys. Res.* 110, B11305. <http://dx.doi.org/10.1029/2004JB003080>.
- Julian, B.R., Gubbins, D., 1977. Three-dimensional seismic ray tracing. *J. Geophys. Res.* 43, 95–113.
- Keller, H.B., Perozzi, D.J., 1983. Fast seismic ray tracing. *SIAM J. Appl. Math.* 43, 981–992.
- Lan, H.Q., Zhang, Z.J., 2013a. Topography-dependent eikonal equation and its solver for calculating first-arrival traveltimes with an irregular surface. *Geophys. J. Int.* 193 (2), 1010–1026. <http://dx.doi.org/10.1093/gji/ggt036>.
- Lan, H.Q., Zhang, Z.J., 2013b. A high-order fast-sweeping scheme for calculating first-arrival travel times with an irregular surface. *Bull. Seismol. Soc. Am.* 103 (3), 2070–2082.
- Langan, R.T., Lerche, I., Cutler, R.T., 1985. Tracing of rays through heterogeneous media: an accurate and efficient procedure. *Geophysics* 50, 1456–1465.
- Maierova, P., Lexa, O., Schulmann, K., Stipska, P., 2014. Contrasting tectono-metamorphic evolution of orogenic lower crust in the Bohemian Massif: a numerical model. *Gondwana Res.* 25 (2), 509–521. <http://dx.doi.org/10.1016/j.gr.2012.08.020>.
- Mallet, J.L., 1989. Discrete smooth interpolation. *ACM Trans. Graph.* 8, 121–144.
- Mallet, J.L., 1992. Discrete smooth interpolation in geometric modeling. *Comput. Aided Des.* 24, 178–193.
- Mao, W.J., Stuart, G.W., 1997. Rapid multi-wave-type ray tracing in complex 2-D and 3-D isotropic media. *Geophysics* 62, 298–308.
- Moser, T.J., 1991. Shortest path calculation of seismic rays. *Geophysics* 56, 59–67.
- Pereyra, V., 1992. Two-point ray tracing in general 3-D media. *Geophys. Prospect.* 40, 267–287.
- Pereyra, V., 1996. Modeling, ray tracing, and block nonlinear travel-time inversion in 3-D. *Pure Appl. Geophys.* 148, 345–386.
- Prothero, W., Taylor, W., Eickemeyer, J., 1988. A fast, two-point, three-dimensional ray-tracing algorithm using a simple step search method. *Bull. Seismol. Soc. Am.* 78, 1190–1198.
- Psencik, I., Teles, T.N., 1996. Point source radiation in inhomogeneous anisotropic structures. *PAGEOPH* 148, 591–623.
- Ravve, I., Koren, Z., 2007. Conic velocity model. *Geophysics* 72, U31–U46.
- Rawlinson, N., Houseman, G.A., Collins, C.D.N., 2001. Inversion of seismic refraction and wide-angle reflection traveltimes for three-dimensional layered crustal structure. *Geophys. J. Int.* 145, 381–400.
- Sambridge, M., Braun, J., McQueen, H., 1995. Geophysical parameterization and interpolation of irregular data using natural neighbours. *Geophys. J. Int.* 122, 837–857.
- Slotnick, M.M., 1936. On seismic computations, with applications. Part I: *Geophysics* 1, 9–22 and Part II. *Geophysics* 1, 299–305.
- Sun, Y., 1993. Ray tracing in 3-D media by parametrized shooting. *Geophys. J. Int.* 114, 145–155.
- Thurber, C.H., 1983. Earthquake locations and three-dimensional crustal structure in the Coyote Lake area, central California. *J. Geophys. Res.* 88, 8226–8236.
- Thurber, C., Ellsworth, W., 1980. Rapid solution of ray tracing problems in heterogeneous media. *Bull. Seismol. Soc. Am.* 70, 1137–1148.
- Um, J., Thurber, C., 1987. A fast algorithm for two-point seismic ray tracing. *Bull. Seismol. Soc. Am.* 77, 972–986.
- Velis, D.R., Ulrych, T.J., 1996. Simulated annealing two-point ray tracing. *Geophys. Res. Lett.* 23, 201–204.
- Velis, D.R., Ulrych, T.J., 2001. Simulated annealing ray tracing in complex three-dimensional media. *Geophys. J. Int.* 145, 447–459.
- Vidale, J.E., 1988. Finite-difference calculation of traveltimes. *Bull. Seismol. Soc. Am.* 78, 2062–2076.
- Vidale, J.E., 1990. Finite-difference calculations of traveltimes in three dimensions. *Geophysics* 55, 521–526.
- Vinje, V., Iverson, E., Gjøystdal, H., 1993. Traveltime and amplitude estimation using wavefront construction. *Geophysics* 58, 1157–1166.
- Vinje, V., Iverson, E., Åstebol, K., Gjøystdal, H., 1996. Estimation of multivalued arrivals in 3D models using wavefront construction – part 1. *Geophys. Prospect.* 44, 819–842.
- Virieux, J., Farra, V., 1991. Ray tracing in 3-D complex isotropic media: an analysis of the problem. *Geophysics* 56, 2057–2069.
- Xu, T., Xu, G., Gao, E., Li, Y., Jiang, X., Luo, K., 2006. Block modeling and segmentally iterative ray tracing in complex 3D media. *Geophysics* 71, T41–T51.
- Xu, T., Zhang, Z., Zhao, A., Zhang, A., Zhang, X., Zhang, H., 2008. Sub-triangle shooting ray tracing in complex 3D VTI media. *J. Seism. Explor.* 17, 131–144.
- Xu, T., Zhang, Z.J., Gao, E.G., Xu, G.M., Sun, L., 2010. Segmentally iterative ray tracing in complex 2D and 3D heterogeneous block models. *Bull. Seismol. Soc. Am.* 100 (2), 841–850.
- Zelt, C.A., Smith, R.B., 1992. Seismic traveltime inversion for 2-D crustal velocity structure. *Geophys. J. Int.* 108, 16–34.
- Zhang, Z.J., Klemperer, S., 2005. West–east variation in crustal thickness in northern Lhasa block, central Tibet, from deep seismic sounding data. *J. Geophys. Res.* 110, 1–14.
- Zhang, Z.J., Wang, Y.H., 2007. Crustal structure and contact relationship revealed from deep seismic sounding data in South China. *Phys. Earth Planet. Inter.* 165, 114–126.
- Zhang, Z.J., Wang, G.J., Teng, J.W., Klemperer, S., 2000. CDP mapping to obtain the fine structure of the crust and upper mantle from seismic sounding data: an example for the southeastern China. *Phys. Earth Planet. Inter.* 122, 133–146.
- Zhang, Z.J., Lin, G., Chen, J.Y., et al., 2003. Inversion for elliptically anisotropic velocity using VSP reflection traveltimes. *Geophys. Prospect.* 51, 159–166.
- Zhang, Z.J., Badal, J., Li, Y.G., et al., 2005. Crust–upper mantle seismic velocity structure across Southeastern China. *Tectonophysics* 395, 137–157.
- Zhang, Z.J., Xu, T., Zhao, B., Badal, J., 2013. Systematic variations in seismic velocity and reflection in the crust of Cathaysia: new constraints on intraplate orogeny in the South China continent. *Gondwana Res.* 24, 902–917. <http://dx.doi.org/10.1016/j.gr.2012.05.18>.
- Zhao, D., Hasegawa, A., Horiuchi, S., 1992. Tomographic imaging of P and S wave velocity structure beneath northeastern Japan. *J. Geophys. Res.* 97, 19909–19928.
- Zhao, A., Zhang, Z., Teng, G., 2004. Minimum travel time tree algorithm for seismic ray tracing: improvement in efficiency. *J. Geophys. Eng.* 1 (4), 245–251.
- Zhou, B., Greenhalgh, S.A., 1992a. Iterative algorithms for the damped minimum norm, least-squares and constrained problem in seismic tomography. *Explor. Geophys.* 23, 497–505.
- Zhou, B., Greenhalgh, S.A., 1992b. Non-linear inversion traveltime tomography: imaging high-contrast inhomogeneities. *Explor. Geophys.* 23, 459–464.